Desalination and Water Treatment
www.deswater.com
doi: 10.5004/dwt.2023.29572

295 (2023) 105–124
May

Multivariable event-triggered predictive control based on recursive bilinear subspace identification for wastewater treatment processes

Hongbiao Zhou*, Shuaixiang Liu, Jian Ren, Jinlong Zhang, Honghai Li

Faculty of Automation, Huaiyin Institute of Technology, Huai'an 223003, China, Tel.: +86-15189544918; emails: hyitzhb@hyit.edu.cn (H. Zhou), 617903095@qq.com (S. Liu), 737052481@qq.com (J. Ren), 2260525119@qq.com (J. Zhang), lihonghai@hyit.edu.cn (H. Li)

Received 5 December 2022; Accepted 17 April 2023

ABSTRACT

To address the issue of precise control of dissolved oxygen (DO) concentration and nitrate nitrogen level in wastewater treatment processes (WWTPs) under the premise of low energy consumption, a multivariable event-triggered model predictive control (ETMPC) strategy based on recursive bilinear subspace identification (RBSI) is proposed in this paper. Since WWTPs have strong non-linear, multivariable coupling and large delay characteristics, the RBSI algorithm with a forgetting factor is used to build the model predictive control (MPC) in this paper. In RBSI-ETMPC, first, to overcome the difficulties in establishing an accurate mathematical model due to the complex reaction mechanism in WWTPs, the BSI algorithm with linear and non-linear advantages and the RBSI algorithm with adaptive updating of parameters are utilized to establish the state space identification model of the wastewater biochemical reaction process. Then, the RBSI predictor equation obtained by the data-driven method is utilized as the MPC prediction model. Under the condition of meeting the event triggering strategy, the sequential quadratic programming algorithm is adopted to solve the quadratic performance function and update the control input at the next time. Finally, four experimental verifications under three working conditions, including a constant setpoint, variable setpoint and variable setpoint with input or output pulse interference, are carried out using international benchmark simulation model no. 1. The experimental results demonstrate that the values of the integral of absolute error, integral of square error and maximal deviation from setpoint of the RBSI-ETMPC decreased by 82.81%, 96.62% and 71.89%, respectively, for the variable setpoint control of the DO concentration under rain weather conditions compared with the recursive linear subspace identification (RLSI)-MPC. Furthermore, the longest trigger interval of the proposed RBSI-ETMPC is 0.8 h, which can save considerable computing resources.

Keywords: Wastewater treatment processes; Recursive bilinear subspace identification; Multivariable control; Model predictive control; Event-triggered scheme

1. Introduction

Wastewater treatment processes (WWTPs) can purify wastewater and maintain freshwater resources, which effectively alleviate the contradiction between urban freshwater supply and demand [1]. Since the main pollutants of wastewater are easily degradable organic matter, aerobic biological treatment methods are adopted in most wastewater treatment plants. Among these methods, the activated sludge process (ASP) is one of the most mature processes [2]. The flow of ASP is composed of primary treatment, secondary treatment and tertiary treatment. Secondary treatment, also known as biochemical treatment, is the main process of an activated sludge WWTP. Secondary treatment generally includes biochemical reaction tanks, secondary sedimentation tanks, sludge return systems, and excess sludge discharge systems. The main task of secondary treatment is to remove colloidal and dissolved organic pollutants and plant nutrients in wastewater

* Corresponding author.

by a large margin. The biochemical reaction tank is divided into an aerobic tank and an anaerobic tank. The biological treatment process of wastewater is carried out in the biochemical reaction tank, which uses the organic matter of wastewater as the nutrient for microorganisms. With the help of biological oxidation, decomposition and transformation functions, the microbial metabolism process is carried out in an artificially created controllable reaction environment to degrade and convert pollutants in wastewater to achieve wastewater purification [3]. To ensure the effect of wastewater treatment, it is necessary to use the blower and lift pump for aeration and reflux operations to control the dissolved oxygen (DO) concentration in the aerobic tank and the nitrate nitrogen (NN) level in the anaerobic tank at the predetermined expected value.

At present, the control methods of the bottom loop in WWTPs are mainly divided into two categories: the first category is post-control methods, and the second category is pre-control methods. The former mainly includes switch control, Proportional-Integral-Derivative (PID) control [4,5], fuzzy logic control (FLC) [6], neural network direct control [7], decoupling control [8], auto disturbance rejection control [9], model free adaptive control [10], and adaptive sliding mode control [11]. However, since WWTP is a typical complex process industrial system, its internal biochemical reaction has serious non-linearity, greater uncertainty, multivariable coupling, and longtime lag, the switch control accuracy is low, the control parameter tuning of PID is difficult, and the post-controller that does not rely on the model has difficulty achieving a satisfactory control effect, and cannot meet the increasingly stringent wastewater discharge standards. The latter mainly includes model predictive control (MPC). MPC decomposes the optimal control problem into several short time spans over a longtime span, which is essentially an optimal controller. MPC can well handle multivariable and multi-constrained industrial process control problems [12].

Over the past two decades, many researchers have devoted themselves to using MPC to solve the control problem of WWTPs. Holenda et al. [13] used a sufficiently low sampling time to capture the dynamic characteristics of the system and built a continuous time state space prediction model to achieve constant value control and step change control of DO. Brdys et al. [14] adopted the grey box model of the biochemical reaction process as a prediction model and designed a layered control framework for DO from three different time scales: slow, medium and fast. Shen et al. [15] constructed an MPC controller based on a quadratic dynamic matrix and used the nonlinear quadratic programming algorithm (NLPQL) method to find the non-linear solution of the control rate. Mulas et al. [16] utilized a dynamic matrix predictive control strategy to achieve online control of effluent ammonia nitrogen concentration. Shen et al. [17] designed a linear dynamic matrix control strategy and a quadratic dynamic matrix control strategy to achieve accurate control of ammonia nitrogen concentration in WWTPs. However, the prediction models relied on by the above MPC controllers are mainly linear models, where their parameters are generally not adjusted in the control process. Thus, it is difficult to accurately describe the non-linear mapping relationship between the inputs and outputs in WWTPs. In addition, control quantities should be calculated at each execution step in the above MPC controllers, which inevitably wastes computational resources.

During the past two decades, compared with time-driven MPC, event-triggered MPC has aroused great interest among researchers. In the application of time-driven control, continuous signals are sampled at evenly spaced measurement times, and control signals are applied to the controlled object in a periodic manner. However, strict periodic control is generally not required in practical engineering applications. Therefore, computing resources are wasted in time-driven control. To improve computational efficiency and save limited computing resources, researchers have proposed a variety of event-triggered MPCs. Boruah and Roy [18] proposed an event-triggered non-linear model predictive control (ETNMPC) controller based on a simplified system model to achieve the control of DO and NN in WWTPs. The triggering condition of ETNMPC is constructed using the deviation of error. Compared with a traditional NMPC and PI controller, the proposed ETNMPC can enhance effluent quality and reduce computational burden. Du et al. [19] developed a fourth-order state space model as the prediction model and constructed an event-triggered model predictive control (ETMPC) controller for DO and NN in WWTPs. The system output error and the predicted step are utilized to develop the triggering mechanism. Compared with MPC, the number of control updates for ETMPC is reduced by up to 60%. Han et al. [20] considering that the delay interference caused by hydraulic retention time would reduce the control accuracy of DO concentration, Han et al. [20] proposed an event-triggered recursive least squares-based sliding mode control (ETRLS-SMC) method with delay disturbance variables. The above-mentioned event-triggered MPC controllers do not need to calculate the control quantity at each execution step. In other words, the control quantity is calculated only when certain triggering conditions are met. In principle, event-triggered MPC can yield more accurate sampling and control actions, saving computing and communication resources.

Furthermore, considering the strong non-linear system identification ability of neural networks, researchers proposed a variety of neural network-based MPC controller design methods and used them to solve the control problems in WWTPs. Han & Qiao [21] and Han et al. [22] used self-organizing radial basis function (RBF) neural networks to build prediction models for the control of DO and NN, in which the gradient descent algorithm and multi-objective gradient descent algorithm are adopted to obtain the input sequence of control quantities. Han et al. [23] proposed an MPC controller based on a fuzzy neural network (FNN), where a complex multi-objective optimization algorithm is utilized to obtain the control rate online. Han et al. [24] presented a hierarchical MPC controller using two FNNs to control DO and NN, where an adaptive gradient descent algorithm is used to acquire the control rate. The above neural network-based MPC controllers with stronger non-linear mapping ability can obviously provide higher prediction accuracy. However, solving the control rate efficiently is still a challenging problem for non-linear MPC.

At present, the data-driven subspace identification method is still one of the most widely used modelling methods for complex industrial systems with complex reaction

mechanisms as it is difficult to establish accurate mathematical models for these systems [25–27]. The principle of the subspace identification method is to use the input and output data of the system to construct a Hankel matrix and use state estimation technology, orthogonal triangular decomposition, singular value decomposition, and the least squares algorithm to establish an identification model without any prior knowledge of the controlled object [28]. In recent years, based on subspace identification methods, researchers have proposed algorithms such as numerical subspace state space system identification (N4SID), linear subspace identification (LSI) and bilinear subspace identification (BSI). These methods have shown superior control performance in blast furnace ironmaking [29], nuclear reactors [30], power grids [31], aeroengines [32], metallurgy bioreactors [33], and other fields. Li et al. [34] proposed a data-driven subspace predictive control method with event triggering and used a 2-tank flow system for experimental verification. Ahmadipour et al. [35] used a subspace identification method based on orthogonal decomposition to identify multi-input multi-output (MIMO) systems with time delays, and the results showed that it can effectively estimate the time delay of the system and the order of the model. Zhou et al. [36] established a prediction model of the blast furnace (BF) ironmaking process using a data-driven subspace identification method, developed a predictive controller to realize hot metal quality control, and used actual industrial field data for performance verification. Patel et al. [37] and Patel et al. [38] utilized a subspace identification approach with first principles-based knowledge to construct a state-space identification model and used a chemical stirred tank reactor process to show superior performance. Ghosh et al. [39], considering the mismatch between the outputs generated by the first-principles model and the plant outputs, Ghosh et al. [39] adopted a subspace model identification algorithm to develop a model for the residuals and addressed the issue of synergizing first-principles models with data-driven models. Experimental results show that the control performance of hybrid MPC is improved and the computational complexity is reduced compared with traditional MPC.

The superiority and effectiveness of subspace predictive control in industrial process control have been verified by the studies described above. However, the complexity of WWTPs makes it difficult for subspace identification methods to achieve satisfactory modelling results. The bilinear subspace, which is an extension of the traditional linear subspace, has both linear and non-linear variable structure characteristics. Since WWTPs are a typical complex process industrial system with severe non-linearity, large uncertainty, multivariable coupling, and long-time delay in its internal biochemical reactions, bilinear subspace identification can accurately describe the system model of WWTPs. To address the above issues, a data-driven recursive bilinear subspace identification method is used to design a prediction model of the event-triggered MPC controller to achieve the accurate tracking control of DO and NN with low energy consumption in WWTPs. The main contributions of this paper are summarized as follows:

- To improve the modelling accuracy, adaptive learning ability and anti-interference ability of the prediction model, a recursive bilinear subspace identification model with an adaptive parameter updating strategy is developed.
- To reduce the number of controller actions while ensuring system performance, an event-trigger mechanism is designed and integrated into MPC controller. Meanwhile, the sequential quadratic programming method is used to solve the quadratic performance index function and obtain the optimal real-time control quantity.
- The international benchmark simulation model no. 1 (BSM1) is used to carry out algorithm performance comparison experiments under different working conditions and different settings, including dry weather, rain weather and storm weather, as well as constant setpoints, variable setpoints, and variable setpoints with pulse interference.

The remainder of this paper is organized as follows. The description of the WWTP is given in Section 2 – Wastewater treatment process. The detailed design process of the RBSI-ETMPC controller is presented in Section 3 – Recursive bilinear subspace identification-event-triggered model predictive control. The effectiveness of RBSI-ETMPC was verified by simulation experiments, as described in Section 4 – Experimental study. Finally, Section 5 concludes this paper.

2. Wastewater treatment process

To facilitate algorithm research, performance comparison and engineering verification of WWTPs, the International Water Quality Association launched the activated sludge benchmark simulation model No. 1 (BSM1). In BSM1, the biochemical reactor is composed of five units, of which unit 1 and unit 2 are anoxic units and unit 3 to unit 5 are aerated units. The anoxic units undertake the nitrification task, while the aerated units undertake the denitrification task. The specific layout of the BSM1 plant is shown in Fig. 1 [40].

BSM1 includes 8 biochemical reaction processes, such as microbial growth, attenuation and hydrolysis, and 13 state variables and follows the following mass balance rule:

$$\left[\text{Input}\right]-\left[\text{Output}\right]+\left[\text{Formation}\right]=\left[\text{Accumulation}\right] \tag{1}$$

where "+" represents material accumulation and "–" represents material consumption. According to Eq. (1), the mass balance equation of each unit is presented as follows:

Unit 1 ($k = 1$):

$$\frac{dZ_1}{dt}=\frac{1}{V_1}\left(Q_aZ_a+Q_rZ_r+Q_0Z_0+r_1V_1-Q_1Z_1\right) \tag{2}$$

$$Q_1=Q_a+Q_r+Q_0 \tag{3}$$

where Z_1 is the concentration of each component in the first unit, V_1 is the volume of the first unit, Q_1 is the flow rate of each component in the first unit, r_1 is the reaction rate of each component in the first unit, Q_a is the internal recycle flow rate, Z_a is the concentration of each component in the internal recycle nitrification liquid, Q_r is the external recycle flow rate, Z_r is the concentration of each component in the sludge refluxing liquid, Q_0 is the influent flow rate, and Z_0 is the concentration of each component in the influent water.

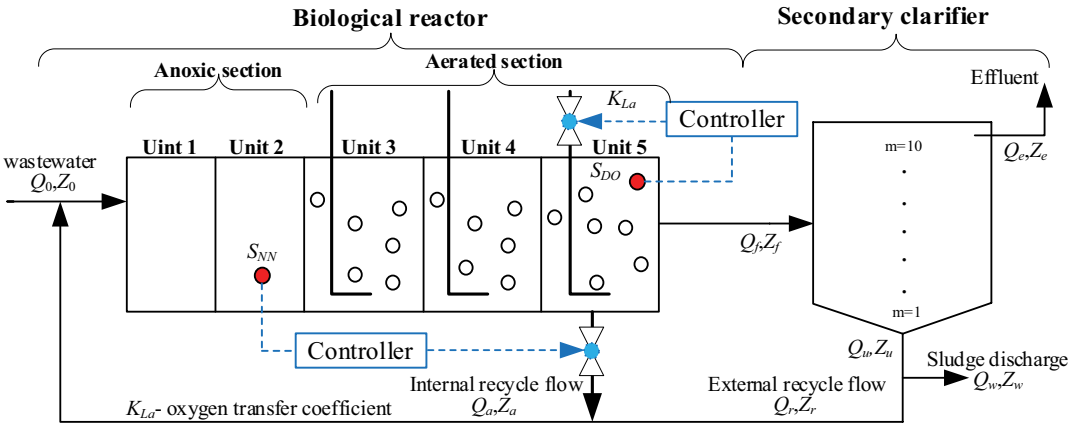

Fig. 1. Layout of the BSM1 plant.

Units 2–5 (k = 2~5):

$$\frac{dZ_k}{dt}=\frac{1}{V_k}\left(Q_{k-1}Z_{k-1}+r_kV_k-Q_kZ_k\right) \tag{4}$$

$$Q_k=Q_{k-1} \tag{5}$$

where Z_k is the concentration of each component in the kth unit, V_k is the volume of the kth unit, Q_k is the flow rate of each component in the kth unit, and r_k is the reaction rate of each component in the kth unit.

The mass balance equation of DO is special, and its change is not only related to the flow rate but also related to the aeration rate. The specific description is given as follows:

$$\frac{dS_{\mathrm{DO},k}}{dt}=\frac{1}{V_k}\begin{pmatrix}Q_{k-1}S_{\mathrm{DO},k-1}+r_kV_k+K_{\mathrm{Lak}}V_k\left(S_{\mathrm{DO,sat}}-S_{\mathrm{DO},k}\right)\\-Q_kS_{\mathrm{DO},k}\end{pmatrix} \tag{6}$$

where $S_{\mathrm{DO},k}$ is the DO concentration of the kth unit, K_{Lak} is the oxygen transfer coefficient of the kth unit, and $S_{\mathrm{DO,sat}}$ is the concentration value when dissolved oxygen is saturated, which is set as $S_{\mathrm{DO,sat}}$ = 8 mg/L.

Other equations are given as follows:

$$Z_a=Z_5 \tag{7}$$

$$Z_f=Z_5 \tag{8}$$

$$Z_w=Z_r \tag{9}$$

$$Q_f=Q_5-Q_a=Q_e+Q_r+Q_w \tag{10}$$

where Z_f and Z_w are the concentrations of each component of the effluent and discharged sludge in the biochemical reactor, respectively, and Q_f, Q_e and Q_w are the effluent flow rate, supernatant flow rate and sludge discharge in the biochemical reactor, respectively.

In the BSM1 model, the volumes V_1 and V_2 of the two anoxic units are 1,000 m^3, and the volumes V_3, V_4 and V_5 of the three aerobic units are 1,333 m^3. From Fig. 1, the bottom layer of BSM1 mainly has two control loops. One controls the DO concentration $S_{\mathrm{DO},5}$ of the fifth unit by adjusting the oxygen transfer coefficient $K_{\mathrm{La},5}$, and the other controls the NN concentration $S_{\mathrm{NN},2}$ of the second unit by adjusting the internal recycle flow rate Q_a. The oxygen transfer coefficients K_{La3} and K_{La4} of the third and fourth units are both set to a constant value of 240 d^{-1}, and the oxygen transfer coefficient K_{La5} of the fifth unit needs to be dynamically adjusted to maintain the DO concentration $S_{\mathrm{DO},5}$ of the fifth unit at a constant value of 2 mg/L. In addition, in the BSM1 model, it is also possible to maintain the NN concentration $S_{\mathrm{NN},2}$ of the second unit by adjusting the internal recycle flow rate Q_a to a constant value of 1 mg/L.

However, WWTPs show strong non-linearity, strong coupling, a large time delay and serious uncertainty due to the complex biochemical reaction mechanism. Thus, the tuning of control parameters is difficult, and the PID control precision needs to be improved [41,42]. Therefore, to realize the low energy consumption control of the water purification process, a recursive bilinear subspace identification (RBSI) algorithm with a forgetting factor is used to build a multivariable event-triggered model predictive controller (ETMPC) for DO and NN in this paper.

3. Recursive bilinear subspace identification-event-triggered model predictive control

To enhance the control accuracy and save control resources, the RBSI-ETMPC is proposed to establish the multivariable controllers of $S_{\mathrm{DO},5}$ and $S_{\mathrm{NN},2}$. In traditional subspace identification, with the increase in the number of row blocks of the Hankel matrix, the computational complexity of the algorithm increases exponentially, which makes it difficult to update the system matrix online. To improve the adaptive learning ability of the model and achieve better prediction accuracy and control performance, the recursive least squares method is introduced to adjust the model parameters online.

3.1. Recursive bilinear subspace identification

3.1.1. Hankel matrix construction

Consider using the following MIMO bilinear system to describe the dynamic change process of $S_{\mathrm{DO},5}$ and $S_{\mathrm{NN},2}$ in WWTPs:

$$x_{t+1} = \mathrm{A}x_t + \mathrm{N}u_t \otimes x_t + \mathrm{B}u_t + K\delta_t \tag{11}$$

$$y_t = \mathrm{C}x_t + \mathrm{D}u_t + \delta_t \tag{12}$$

where $u_t \in R^m$, $y_t \in R^l$, and $x_t \in R^n$ represent the input vector, output vector and state vector of the system, respectively; $\delta_t \in R^l$ represents the zero mean white noise sequence, which has the covariance matrix $E[\delta_t \delta_t^T] = S_{l\times l}$; $K \in R^{n\times l}$ represents the Kalman filter gain; $N \in R^{n\times nm}$ represents the bilinear characteristic matrix of the system; A, B, C and D represent the system matrix, input matrix, output matrix and direct feedback matrix, respectively; and $a \otimes b = [a_1 b^T, a_2 b^T, \ldots, a_p b^T] \in R^{pq}$ represents the Kronecker product of the vector, where $a \in R^p$, $b \in R^q$ [29,36].

According to Eq. (12), the state vector at time t is given as follows:

$$x_t = C^{\dagger}\left(y_t - \mathrm{D}u_t - \delta_t\right) \tag{13}$$

where $C^{\dagger}$ represents the pseudoinverse matrix of C.

Taking Eq. (13) into the Kronecker product of the control vector u_t and the state vector x_t expressed in Eq. (11), the following equation is obtained:

$$f\left(u_t, y_t\right) = u_t \otimes C^{\dagger} y_t - u_t \otimes C^{\dagger}\mathrm{D}u_t - u_t \otimes C^{\dagger}\delta_t \tag{14}$$

Simplifying Eq. (14), we can obtain:

$$f\left(u_t, y_t\right) = \mathrm{Q}u_t \otimes y_t - \mathrm{R}u_t \otimes u_t - u_t \otimes C^{\dagger}\delta_t \tag{15}$$

where diagonal matrices $Q \in R^{mn\times ml}$ and $R \in R^{mn\times mm}$ are respectively expressed as follows:

$$Q = \begin{bmatrix} C^{\dagger} & 0 & 0 & 0 \\ 0 & C^{\dagger} & 0 & 0 \\ 0 & 0 & \ddots & 0 \\ 0 & 0 & 0 & C^{\dagger} \end{bmatrix} \tag{16}$$

$$R = \begin{bmatrix} C^{\dagger}D & 0 & 0 & 0 \\ 0 & C^{\dagger}D & 0 & 0 \\ 0 & 0 & \ddots & 0 \\ 0 & 0 & 0 & C^{\dagger}D \end{bmatrix} \tag{17}$$

Substituting Eq. (15) into Eq. (11), the state vector x at time t+1 can be obtained:

$$\begin{aligned} x_{t+1} = {} & \mathrm{A}x_t + \mathrm{NQ}u_t \otimes y_t - \mathrm{NR}u_t \otimes u_t \\ & + \mathrm{B}u_t + \left(K - \mathrm{N}u_t \otimes C^{\dagger}\right)\delta_t \end{aligned} \tag{18}$$

To simplify the calculation process, some variables in Eq. (18) are defined as follows:

$$\tilde{u}_t = \begin{bmatrix} u_t \\ u_t \otimes y_t \\ u_t \otimes u_t \end{bmatrix} \tag{19}$$

$$\tilde{B} = \begin{bmatrix} B & \mathrm{NQ} & -\mathrm{NR} \end{bmatrix} \tag{20}$$

$$\tilde{K} = \begin{bmatrix} K & -\mathrm{N}u_t \otimes C^{\dagger} \end{bmatrix} \tag{21}$$

Then, Eq. (18) can be rewritten as follows:

$$x_{t+1} = \mathrm{A}x_t + \tilde{B}\tilde{u}_t + \tilde{K}\delta_t \tag{22}$$

Thus, the state space form of the bilinear system can be expressed as:

$$\begin{aligned} x_{t+1} &= \mathrm{A}x_t + \tilde{B}\tilde{u}_t + \tilde{K}\delta_t \\ y_t &= \mathrm{C}x_t + \mathrm{D}u_t + \delta_t \end{aligned} \tag{23}$$

Eq. (23) shows that the bilinear system has the same state space form as the linear state space, but their constituent elements are essentially different. The input of the bilinear system is composed of the input u_t, the Kronecker product of the input and the output $u_t \otimes y_t$, and the Kronecker product of the input and the input $u_t \otimes u_t$. Therefore, it is necessary to consider the effects of different inputs when using linear subspace identification to address the bilinear subspace identification process.

For the bilinear system expressed in Eq. (13), without considering noise interference, Eq. (22) is brought into Eq. (12) for the forwards iterative operation, and the results are written in the following matrix form:

$$\begin{aligned} \begin{bmatrix} y_k & \cdots & y_{k+j-1} \\ \vdots & \ddots & \vdots \\ y_{k+j-1} & \cdots & y_{k+j+i-2} \end{bmatrix} = {} & \begin{bmatrix} C \\ \mathrm{CA} \\ \vdots \\ \mathrm{CA}^{i-1} \end{bmatrix} \begin{bmatrix} x_k & x_{k+1} & \cdots & x_{k+j-1} \end{bmatrix} \\ & + \begin{bmatrix} 0 & \cdots & 0 \\ \vdots & \ddots & \vdots \\ \mathrm{CA}^{i-2}\tilde{B} & \cdots & 0 \end{bmatrix} \begin{bmatrix} \tilde{u}_k & \cdots & \tilde{u}_{k-j-1} \\ \vdots & \ddots & \vdots \\ \tilde{u}_{k+i-1} & \cdots & \tilde{u}_{k+j+i-2} \end{bmatrix} \\ & + \begin{bmatrix} D & \cdots & 0 \\ \vdots & \ddots & \vdots \\ 0 & \cdots & D \end{bmatrix} \begin{bmatrix} u_k & \cdots & u_{k-j-1} \\ \vdots & \ddots & \vdots \\ u_{k+i-1} & \cdots & u_{k+j+i-2} \end{bmatrix} \end{aligned} \tag{24}$$

Eq. (24) can be defined as follows:

$$M_i = \begin{bmatrix} 0 & 0 & \cdots & 0 \\ C\tilde{B} & 0 & \cdots & 0 \\ \vdots & \vdots & \ddots & \vdots \\ \mathrm{CA}^{i-2}\tilde{B} & \mathrm{CA}^{i-3}\tilde{B} & \cdots & 0 \end{bmatrix} \tag{25}$$

$$M_i^d = \begin{bmatrix} D & 0 & \cdots & 0 \\ 0 & D & \cdots & 0 \\ \vdots & \vdots & \ddots & \vdots \\ 0 & 0 & \cdots & D \end{bmatrix} \tag{26}$$

where M_i represents the lower triangular Toeplitz matrix and M_i^d represents a diagonal block matrix. Assuming {*A*,*C*} is observable and {*A*,*B*} is controllable, the generalized observable matrix Γ_i and the generalized controllability matrix Δ_i can be expressed as:

$$\Gamma_i = \begin{bmatrix} C \\ CA \\ \vdots \\ CA^{i-1} \end{bmatrix} \tag{27}$$

$$\Delta_i = \begin{bmatrix} A^{i-1}\tilde{B} & A^{i-2}\tilde{B} & \cdots & \tilde{B} \end{bmatrix} \tag{28}$$

Let k = 0, and the input Hankel matrix blocks are defined as follows:

$$U_p = \begin{bmatrix} u_0 & u_1 & \cdots & u_{j-1} \\ u_1 & u_2 & \cdots & u_j \\ \vdots & \vdots & \ddots & \vdots \\ u_{i-1} & u_i & \cdots & u_{j+i-2} \end{bmatrix} \tag{29}$$

$$U_f = \begin{bmatrix} u_i & u_{i+1} & \cdots & u_{i+j-1} \\ u_{i+1} & u_{i+2} & \cdots & u_{i+j} \\ \vdots & \vdots & \ddots & \vdots \\ u_{2i-1} & u_{2i} & \cdots & u_{j+2i-2} \end{bmatrix} \tag{30}$$

where U_p and U_f represent the input Hankel matrix blocks at the current time and the future time, respectively. Similarly, the output Hankel matrix blocks Y_p and Y_f at the current time and the future time can be defined. In addition, the generalized input Hankel matrix blocks $\tilde{U}_p$ and $\tilde{U}_f$ can be defined by replacing the input vector u with a generalized input vector $\tilde{u}$. The state matrices X_p and X_f are defined as follows:

$$X_p = \begin{bmatrix} x_0 & x_1 & \cdots & x_{j-1} \end{bmatrix} \tag{31}$$

$$X_f = \begin{bmatrix} x_i & x_{i+1} & \cdots & x_{i+j-1} \end{bmatrix} \tag{32}$$

The input and output equations can be obtained as follows:

$$Y_p = \Gamma_i X_p + M_i \tilde{U}_p + M_i^d U_p \tag{33}$$

$$Y_f = \Gamma_i X_f + M_i \tilde{U}_f + M_i^d U_f \tag{34}$$

$$X_f = A^i X_p + \Delta_i \tilde{U}_p \tag{35}$$

3.1.2. Model solution

The input X_p of the system can be obtained by deriving Eq. (33):

$$X_p = \Gamma_i^{\dagger}\left(Y_p - M_i \tilde{U}_p - M_i^d U_p\right) \tag{36}$$

By introducing Eq. (36) into Eq. (35), the future input X_f of the system can be obtained:

$$X_f = \left(\Delta_i - A^i \Gamma_i^{\dagger} M_i\right)\tilde{U}_p - A^i \Gamma_i^{\dagger} M_i^d U_p + A^i \Gamma_i^{\dagger} Y_p \tag{37}$$

By introducing Eq. (37) into Eq. (34), the future output Y_f of the system can be obtained:

$$\begin{aligned} Y_f = {} & \left(\Gamma_i \Delta_i - \Gamma_i A^i \Gamma_i^{\dagger} M_i\right)\tilde{U}_p + M_i \tilde{U}_f \\ & - \Gamma_i A^i \Gamma_i^{\dagger} M_i^d U_p + \Gamma_i A^i \Gamma_i^{\dagger} Y_p + M_i^d U_f \end{aligned} \tag{38}$$

Eq. (38) can be abbreviated as follows:

$$Y_f = L_v W_v + L_p W_p + L_u W_u \tag{39}$$

The parameters in Eq. (39) are defined as follows:

$$\begin{cases} L_v = \begin{bmatrix} \Gamma_i \Delta_i - \Gamma_i A^i \Gamma_i^{\dagger} M_i & M_i \end{bmatrix} \\ W_v = \begin{bmatrix} \tilde{U}_p & \tilde{U}_f \end{bmatrix}^T \\ L_p = \begin{bmatrix} -\Gamma_i A^i \Gamma_i^d M_i^d & \Gamma_i A^i \Gamma_i^{\dagger} \end{bmatrix} \\ W_p = \begin{bmatrix} U_p & Y_p \end{bmatrix}^T \\ L_u = M_i^d \\ W_u = U_f \end{cases} \tag{40}$$

Eq. (40) can be used as the subspace predictor. The RBSI prediction model with an adaptive update scheme is expressed as:

$$\hat{y}_f = \hat{L}_v w_v + \hat{L}_p w_p + \hat{L}_u w_u \tag{41}$$

To realize the adaptive updating of model parameters, the recursive least squares algorithm with forgetting factor (RLS-FF) is used to estimate the values of $\hat{L}_v$, $\hat{L}_p$ and $\hat{L}_u$, as follows:

$$\hat{L}_{k+1} = \hat{L}_k + v_{k+1}\left(y_{k+1}^T - \varphi_{k+1}^T \hat{L}_k\right) \tag{42}$$

$$v_{k+1} = p_k \varphi_{k+1}\left(\lambda + \varphi_{k+1}^T P_k \varphi_{k+1}\right)^{-1} \tag{43}$$

$$P_{k+1} = \frac{\left(I - v_{k+1}\varphi_{k+1}^T\right)P_k}{\lambda} \tag{44}$$

where $\hat{L}_k = \begin{bmatrix} \hat{L}_{\mathrm{kp}}, \hat{L}_{\mathrm{ku}}, \hat{L}_{\mathrm{kv}} \end{bmatrix}^T$ represents the subspace matrix parameter matrix at time k, $\varphi_k = \begin{bmatrix} w_{\mathrm{kp}}^T, w_{\mathrm{ku}}^T, w_{\mathrm{kv}}^T \end{bmatrix}$ represents the input and output data vector at time k, v_k represents the gain vector, P_k represents the covariance matrix, and λ represents the forgetting factor.

3.2. Event-triggered model predictive control

Fig. 2 shows the architecture diagram of RBSI-ETMPC, which is mainly composed of an RBSI-based prediction

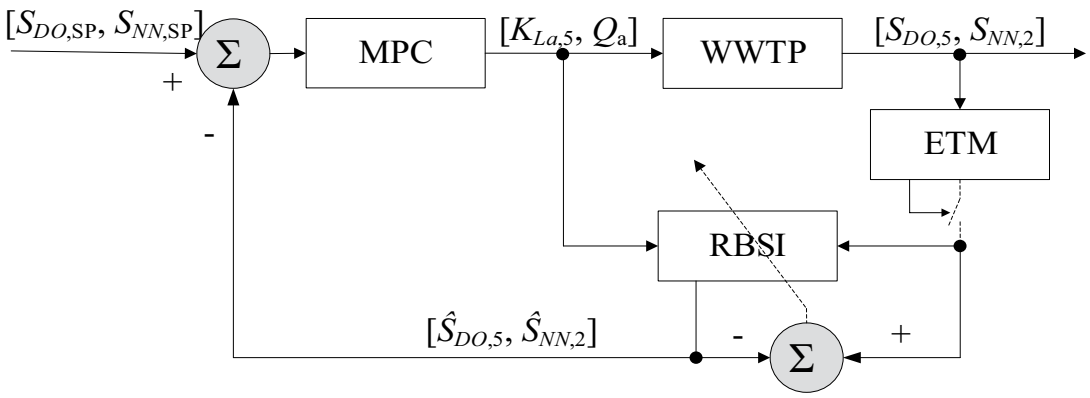

Fig. 2. Architecture of RBSI-ETMPC.

model, an adaptive update mechanism of model parameters, feedback correction, rolling optimization and an event-triggering mechanism. From Fig. 2, the controlled variables are the DO concentration in the fifth unit ($S_{DO,5}$) and the NN concentration in the second unit ($S_{NN,2}$). Correspondingly, the manipulated variables are the oxygen transfer coefficient in the fifth unit (K_{La5}) and the internal recycle flow rate (Q_a). The proposed RBSI-ETMPC is used to obtain optimal $K_{La,5}$ and Q_a to control $S_{DO,5}$ and $S_{NN,2}$ to track the setpoints [$S_{DO,sp}$, $S_{NN,sp}$]. The ETM can effectively reduce the number of controller actions while ensuring excellent control performance of the system [41,42].

3.2.1. Prediction model

The RBSI algorithm proposed in Section 2.1 is used to establish the prediction model of $S_{DO,5}$ and $S_{NN,2}$, where the input variables are $K_{La,5}$ and Q_a, respectively, and the output variables are $S_{DO,5}$ and $S_{NN,2}$. According to Eqs. (32)–(34), the estimated values of the subspace matrices $\hat{L}_v$, $\hat{L}_p$ and $\hat{L}_u$ can be obtained, and the RBSI prediction model is obtained by substituting them into Eq. (31).

3.2.2. Event-triggering mechanism

Since the traditional MPC controllers of DO and NN need to solve the quadratic programming problem at each iteration step, the calculation burden is large. In this paper, an event-triggering mechanism is designed. Only when the event-triggering conditions are met should the control input at the next time be updated using the sequential quadratic programming (SQP) method. The proposed ETM effectively reduces the number of controller actions and saves the energy consumption required for aeration and pumping.

The ETM is mainly composed of an event generator, buffer area, and controller [18,19]. The event generator is utilized to monitor whether a trigger event is formed. The control sequence of the last time is stored in the buffer area. When the control strategy is triggered, the SQP method is used to calculate the control input at the next time by the controller. Otherwise, the next control quantity of the control sequence in the buffer area will continue to be used as the next control input. The trigger strategy is designed as follows:

$$\left|Y_{\text{set}}(t)-\hat{y}(t)\right|\geq\beta \text{ or } \left\{J=\left\lceil\Delta u(t)\right\rceil\right\}>N_c \tag{45}$$

where $y_{set}(t)$ and $\hat{y}(t)$ are the setpoint and the actual output value of the controlled variable at time t, respectively, β is the threshold of control error, J is the index of the current control increment $\Delta u(t)$ in the control sequence, and N_c is the control length of the control increment $\Delta u(t)$. Obviously, the smaller the value of β is, the higher the probability of the ETM being triggered; conversely, the higher the value of β is, the smaller the chance of the ETM being triggered. A value of N_c that is too small may result in control failure; conversely, an excessively high value of N_c will cause significant computational overhead.

3.2.3. Rolling optimization

The control rate of MPC is acquired by solving the rolling optimization problem in the finite time domain, which is defined as follows:

$$\begin{aligned}\min_u = &\sum_{K=1}^{N_p}\left(y_r(t+k)-y_p(t+k)\right)^T Q\left(y_r(t+k)-Y_p(t+k)\right)\\ &+\sum_{K=1}^{N_c}\Delta u(t+k)^T R\Delta u(t+k)\end{aligned} \tag{46}$$

where $y_r(t+k)$ and $y_p(t+k)$ are the predicted output and the expected output at time $t+k$, respectively, $\Delta u(t+k)$ is the control increment at time $t+k$, N_p and N_c are the prediction horizon and the control horizon, respectively, and Q and R are weighted positive matrices on tracking error and control increment, respectively. In the developed MPC, the oxygen transfer coefficient K_{La5} in the fifth unit and the internal circulation flow rate Q_a are considered as control input u, while the DO concentration in the fifth unit $S_{DO,5}$ and the NN concentration in the second unit $S_{NN,2}$ are considered as controlled output y.

In this paper, the SQP algorithm is adopted to solve the quadratic performance index given in Eq. (46). In the traditional MPC, only the first control increment $\Delta u(t+1)$ in a group of control sequences obtained is applied to the controlled object (described in Eqs. (11) and (12)) to

ensure the timeliness of control. For the designed ETMPC in this paper, only the event-trigger conditions are met, and the rolling optimization algorithm is used to obtain the control increment $\Delta u(t+k)$. If no control action is triggered in some control steps, the control increment in the previous control sequence will be used as the current control increment $\Delta u(t)$ in turn.

3.2.4. Feedback correction

Due to the problems of interference and model mismatch in WWTPs, the error of the prediction model will gradually increase with the reaction. If the model output is not corrected in time, the prediction model will be unable to identify the dynamic response process, resulting in model failure. To acquire the ideal control effect, feedback correction is usually used to correct the output of the predictive model in MPC. The methods of feedback correction mainly are mainly the compensation method and online correction method. To improve the accuracy of the prediction model, these two correction methods are comprehensively used to design the feedback correction link in this paper [28,35]. The compensation scheme for the prediction output is presented as follows:

$$\begin{cases} e(t) = y(t) - y_m(t) \\ y_p(t+k) = y_f(t+k) + \alpha e(t) \end{cases} \tag{47}$$

where $y(t)$ is the real output of the controlled object at time t, $y_m(t)$ is the predicted output of the predictive model at time t, $y_f(t+k)$ is the output of the non-linear predictor at time $t+k$, and $y_p(t+k)$ is the model corrected output of the controlled object at time $t+k$. α is the compensation coefficient, which can be set and adjusted according to the actual control effect. In the proposed RBSI-ETMPC, the recursive least squares algorithm with a forgetting factor is used to modify the model parameters online according to the latest input and output data while compensating for the output of the prediction model.

3.3. Algorithm process

The algorithm flow of the RBSI-ETMPC is described in Algorithm 1. First, the RBSI model is built in Steps 1–3. Then, the process data are used to train the model and test its predictive performance in Step 4. During the real-time control process described in Steps 5–7, the controller needs to continuously detect whether the ETM is triggered. If the ETM is triggered, the SQP algorithm is used to solve the performance index function to obtain real-time control quantities. Otherwise, the next control quantity is obtained directly from the control sequence without complex calculations. To adapt to the dynamic changes of the system, it is also necessary to update the parameters of the RBSI model in real time in Step 8. Steps 5–8 are repeatedly executed until the entire control process is completed.

Algorithm 1: RBSI-ETMPC

Step 1: Construct the Hankel data matrices for input U and output Y;
Step 2: Estimate the values of the subspace matrix according to Eqs. (42)–(44);
Step 3: Establish the RBSI-based prediction model according to Eq. (41);
Step 4: Train and test the model, and adjust the parameters of the model if necessary;
Step 5: Judge whether the ETM is triggered according to Eq. (45);
Step 6: Solve the rolling optimization problem using SQP algorithm if the ETM is triggered;
Step 7: Execute the next control increment in the control sequence if the ETM is not triggered;
Step 8: Update the parameters of RBSI model using RLS algorithm according to Eqs. (42)–(44);
Step 9: If stopping conditions are met, then stop. Otherwise, go to Step 5.

The flow chart of the RBSI-ETMPC is shown in Fig. 3.

4. Experimental study

4.1. Experimental data

The predictive control performance of the designed RBSI-ETMPC is verified using the BSM1 platform in this paper. The acquisition duration of the experimental data is 14 d. The variation ranges of the oxygen transfer coefficient $K_{La,5}$ and the internal recycle flow rate Q_a are [0, 240 d^{-1}] and [0, 92,230 m^3/d], respectively. The data mainly include dry weather, rain weather and storm weather. The performance of the RBSI-ETMPC algorithm is verified on the 8th to 12th days since these 3 d have obvious weather changes. The random step changes of $K_{La,5}$ and Q_a are used to obtain the corresponding data samples of $S_{DO,5}$ and $S_{NN,2}$. The changes of $S_{DO,5}$ and $S_{NN,2}$ under the three working conditions are irregular since step changes are used. A total of 960 data samples were collected using BSM1. Fig. 4 shows the change trends of $K_{La,5}$, Q_a, $S_{DO,5}$ and $S_{NN,2}$ under the three working conditions.

To make the training dataset reflect the characteristics of different working conditions as much as possible, the 960 samples collected are divided into 192 groups which with 5 samples in each group. The first three observations of each group are selected as the training dataset, and the last two observations are chosen as the testing dataset. Therefore, there are 576 training samples and 384 testing samples.

4.2. Performance index

To fairly compare the performance of different controllers, three indicators, including the integral of absolute error (IAE), integral of square error (ISE) and maximal deviation from setpoint (DEV^{max}), are defined in the BSM1 model. Their expressions are given as follows:

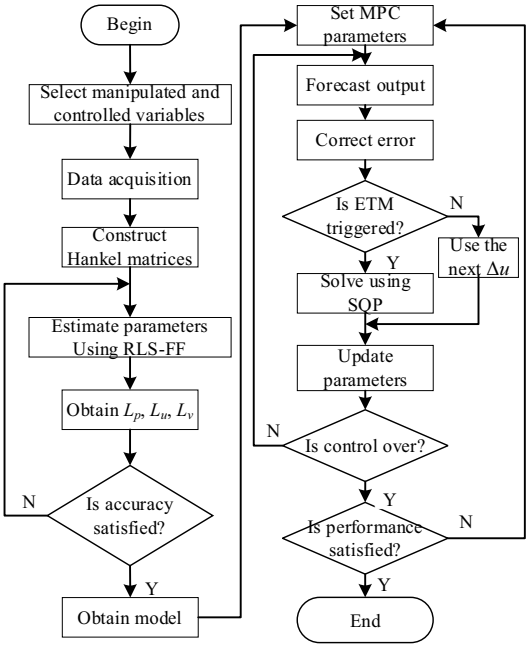

Fig. 3. Flow chart of the RBSI-ETMPC algorithm.

$$\mathrm{IAE} = \frac{\int_{5h}^{25h} |e| dt}{n} \tag{48}$$

$$\mathrm{ISE} = \frac{\int_{5h}^{25h} e^2 dt}{n} \tag{49}$$

$$\mathrm{Dev}^{\max} = \max\{|e|\} \tag{50}$$

where e represents the error between the setpoint and the true value. IAE, ISE and $\mathrm{DEV}^{\max}$ can reflect the transient response, stability and anti-interference ability of the control system, respectively.

4.3. Result analysis

4.3.1. RBSI model validation (Experiment 1)

To verify the identification capability of the RBSI model, simulation tests are conducted using the real data of dry weather, rain weather and storm weather. Fig. 5 shows the comparison of the prediction results between the RBSI model and the recursive linear subspace identification (RLSI) model. From Fig. 5, the RBSI model has a superior prediction accuracy over the RLSI model. Thus, the RBSI

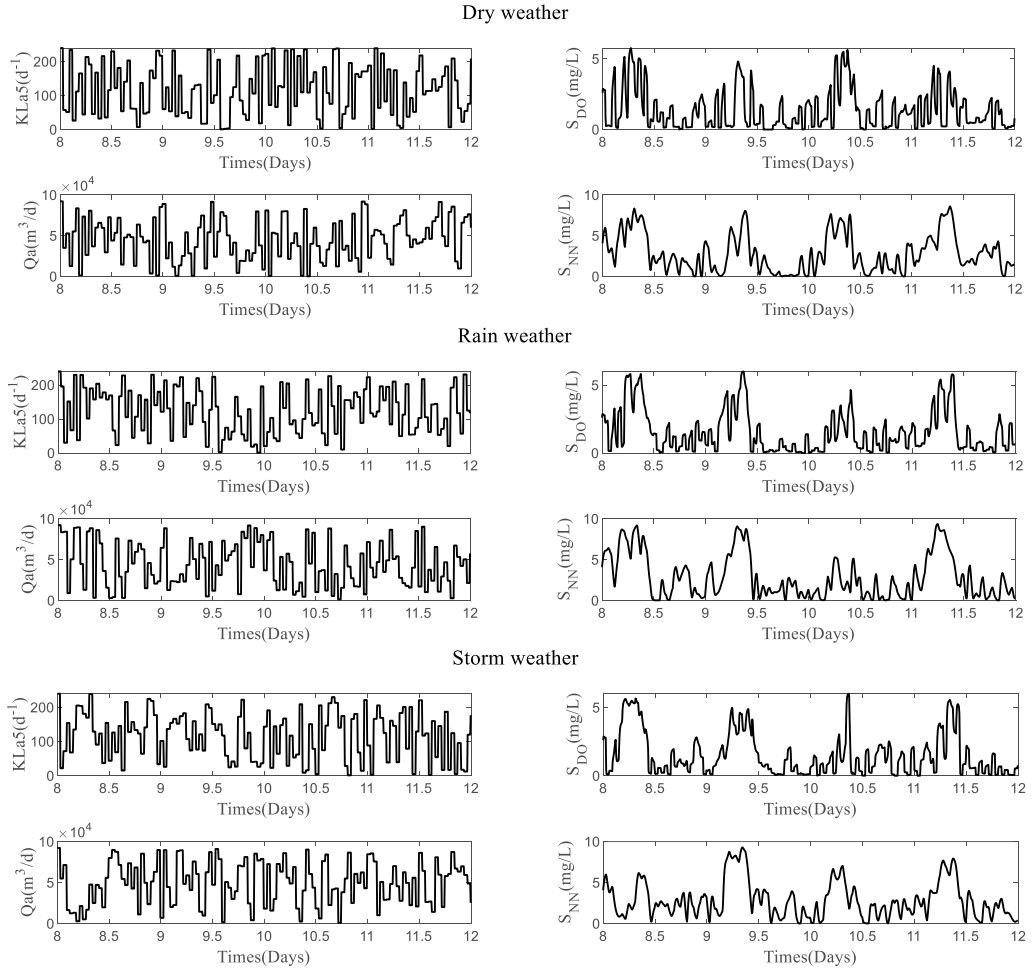

Fig. 4. Change trends of $K_{\mathrm{La},5}$, Q_a, $S_{\mathrm{DO},5}$, and $S_{\mathrm{NN},2}$ under three working conditions.

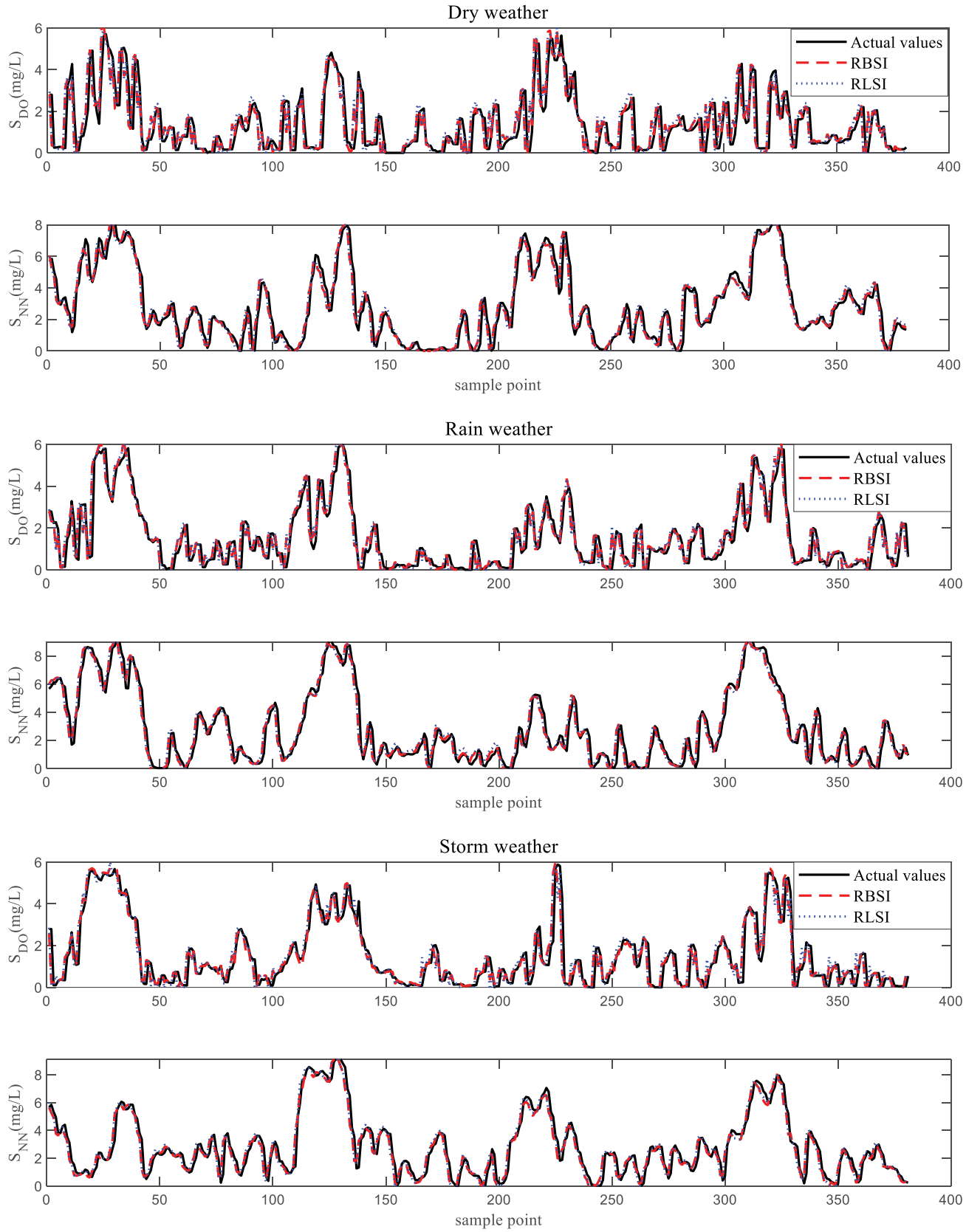

Fig. 5. Test results of the RBSI and RLSI models under three working conditions.

model is effective enough to establish prediction models for $S_{DO,5}$ and $S_{NN,2}$.

To more clearly show the prediction results of the RBSI, the RMSE values of RBSI, RLSI and LSI are given in Table 1. Compared with the RLSI and LSI, the proposed RBSI has a smaller RMSE value, which indicates that it has better prediction accuracy. For example, compared with the LSI, the prediction accuracy of RBSI for $S_{DO,5}$ and $S_{NN,2}$ in storm weather is improved by 8.42% and 8.40%, respectively. The modelling results demonstrate that the bilinear system and recursive strategy can address the strong non-linear changes caused by complex working conditions and enhance the prediction accuracy of the model.

4.3.2. Constant setpoint control (Experiment 2)

In the experiment with constant setpoint control for the WWTP, the concentrations of $S_{DO,5}$ and $S_{NN,2}$ are set to 2 and 2.5 mg/L, respectively. The time range of constant setpoint control is 0–25 h. The control parameters of the RBSI-ETMPC are set as follows: prediction horizon N_p = 10, control horizon N_c = 10, error weighting matrix $Q = 15 \times I_{2\times2}$, compensation coefficient α = 0.92, softening coefficient γ = 0.06, and initial covariance matrix $P = 10^6 \times I_{14\times14}$. Under dry weather conditions, the control weighting matrix $R = 0.001 \times I_{2\times2}$, and the forgetting factor λ = 1. Under rainy weather and storm weather conditions, the control weighting matrix $R = 0.013 \times I_{2\times2}$, and the forgetting factor λ = 0.98.

Fig. 6 demonstrates the control performance of the RBSI-ETMPC controller with constant setpoints under three working conditions. Fig. 6 shows that RBSI-ETMPC has small overshoot and high control accuracy. The results show that RBSI-ETMPC can adapt to different working conditions. Compared with RBSI-ETMPC, RLSI-MPC has difficulty tracking the setpoints in the initial control stage, and there is also a large control deviation during the control process. Meanwhile, the longest trigger interval of the RBSI-ETMPC is 0.6 h, which shows that the event trigger strategy can reduce the number of control actions.

To demonstrate the advantages of the developed RBSI-ETMPC, Table 2 shows the values of the IAE, ISE and DEV^{max} for different control strategies under three working conditions. Compared with RLSI-MPC and LSI-MPC, the proposed RBSI-ETMPC has the best IAE, ISE and DEV^{max}. Taking dry weather conditions as an example, for the control of $S_{DO,5}$, compared with RLSI-MPC, the values of IAE, ISE and DEV^{max} of RBSI-ETMPC decreased by 92.91%, 99.00% and 68.14%, respectively. For the control of $S_{NN,2}$, compared with RLSI-MPC, the values of IAE, ISE and DEV^{max} of RBSI-ETMPC decreased by 56.12%, 72.10% and 19.23%, respectively. Table 2 shows that the proposed RBSI-ETMPC has superior control performance.

Table 1
RMSE values of different models under three working conditions

Working condition	Model	RMSE of $S_{DO,5}$ (mg/L)	RMSE of $S_{NN,2}$ (mg/L)
Dry weather	RBSI	0.8697	0.6820
	RLSI	0.8834	0.6914
	LSI	1.0470	0.6538
Rain weather	RBSI	0.6428	0.6896
	RLSI	0.6620	0.6933
	LSI	0.7642	0.6345
Storm weather	RBSI	0.5852	0.6301
	RLSI	0.6351	0.6406
	LSI	0.6390	0.6879

4.3.3. Variable setpoint control (Experiment 3)

In the variable setpoint control experiment for the WWTP, the concentration of $S_{DO,5}$ is set to 2, 2.1 and 2 mg/L in the ranges of 0~5 h, 5~15 h and 15~25 h, respectively. The concentration of $S_{NN,2}$ is set to 2.5, 2.6 and 2.5 mg/L within the ranges of 0~10 h, 10~20 h and 20~25 h, respectively. The control parameter settings of RBSI-ETMPC in this experiment are the same as those in Experiment 2.

The control results of the RBSI-ETMPC controller with variable setpoints under three working conditions are represented in Fig. 7. From Fig. 7, it takes a long time (approximately 5 h) for RLSI-MPC to track the setpoints under the three working conditions. Compared with RLSI-MPC, the proposed RBSI-ETMPC not only has a short rise time and small overshoot but also has high steady-state control accuracy. In particular, when the setpoints change step by step, RBSI-ETMPC can quickly respond to the change to stabilize the system output near the setpoints in a short time. Under the complex working conditions of rain weather and storm weather, RBSI-ETMPC has a slight oscillation phenomenon for the control of $S_{NN,2}$ due to the introduction of the event-triggering strategy. However, under the action of the event-triggering strategy, the developed RBSI-ETMPC effectively save the control resources while ensuring the control quality. The longest trigger interval is 0.8 h, showing that the energy consumption can be effectively reduced.

Table 3 shows the values of the IAE, ISE and DEV^{max} for different control strategies. Compared with RLSI-MPC and LSI-MPC, the proposed RBSI-ETMPC has a smaller IAE, ISE and DEV^{max} under the three working conditions, which indicates that it can adapt well to the variable setpoints. Taking rain weather conditions as an example, for the control of $S_{DO,5}$, compared with RLSI-MPC, the values of IAE, ISE and DEV^{max} of RBSI-ETMPC decreased by 82.81%, 96.62% and 71.89%, respectively. For the control of $S_{NN,2}$, compared with RLSI-MPC, the values of IAE of RBSI-ETMPC decreased by 13.31%. Due to the introduction of the event-triggering mechanism, the values of ISE decreased slightly, and the values of DEV^{max} increased slightly.

4.3.4. Variable setpoint control with input pulse interference (Experiment 4)

In the experiment of variable setpoint control with input pulse interference for the WWTP, the settings of the concentration of $S_{DO,5}$ and the level of $S_{NN,2}$ are the same as those in Experiment 2. However, input pulse interferences are added to K_{La5} at 6 h and to Q_a at 15 h. The control parameter settings of the RBSI-ETMPC in this experiment are the same as those in Experiment 2.

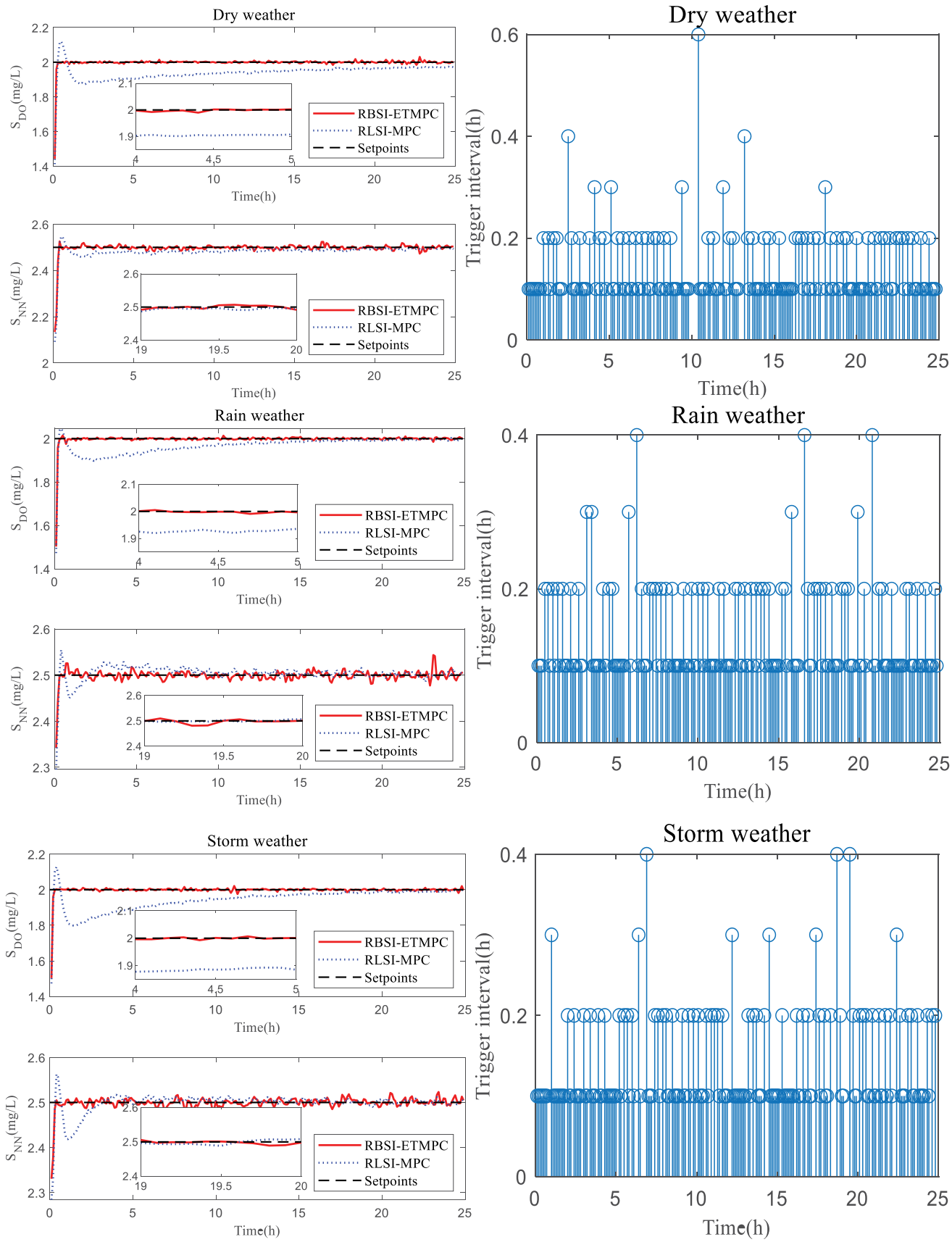

Fig. 6. Control effects of RBSI-ETMPC with constant setpoints under three working conditions.

Table 2
Control accuracy of different control strategies with constant setpoints under three working conditions

Working condition	Variable	Controller	IAE (mg/L)	ISE (mg/L)	DEV^{max} (mg/L)
Dry weather	$S_{DO,5}$	RBSI-ETMPC	3.65×10^{-3}	2.88×10^{-5}	3.10×10^{-2}
		RLSI-MPC	5.15×10^{-2}	3.00×10^{-3}	9.73×10^{-2}
		LSI-MPC	8.49×10^{-2}	1.14×10^{-2}	2.61×10^{-1}
	$S_{NN,2}$	RBSI-ETMPC	5.66×10^{-3}	5.86×10^{-5}	2.73×10^{-2}
		RLSI-MPC	1.29×10^{-2}	2.10×10^{-4}	3.38×10^{-2}
		LSI-MPC	7.48×10^{-2}	1.36×10^{-2}	3.61×10^{-1}
Rain weather	$S_{DO,5}$	RBSI-ETMPC	3.05×10^{-3}	1.49×10^{-5}	1.51×10^{-2}
		RLSI-MPC	2.04×10^{-2}	7.30×10^{-4}	7.65×10^{-2}
		LSI-MPC	3.54×10^{-2}	2.95×10^{-3}	1.59×10^{-1}
	$S_{NN,2}$	RBSI-ETMPC	5.88×10^{-3}	6.56×10^{-5}	4.37×10^{-2}
		RLSI-MPC	6.34×10^{-3}	6.70×10^{-5}	2.50×10^{-2}
		LSI-MPC	1.30×10^{-2}	2.67×10^{-4}	4.80×10^{-2}
Storm weather	$S_{DO,5}$	RBSI-ETMPC	3.48×10^{-3}	2.71×10^{-5}	2.45×10^{-2}
		RLSI-MPC	3.64×10^{-2}	2.09×10^{-3}	1.15×10^{-1}
		LSI-MPC	5.09×10^{-2}	5.15×10^{-3}	2.04×10^{-1}
	$S_{NN,2}$	RBSI-ETMPC	5.92×10^{-3}	5.75×10^{-5}	2.34×10^{-2}
		RLSI-MPC	5.20×10^{-3}	4.10×10^{-5}	1.70×10^{-2}
		LSI-MPC	1.39×10^{-2}	3.33×10^{-4}	3.89×10^{-2}

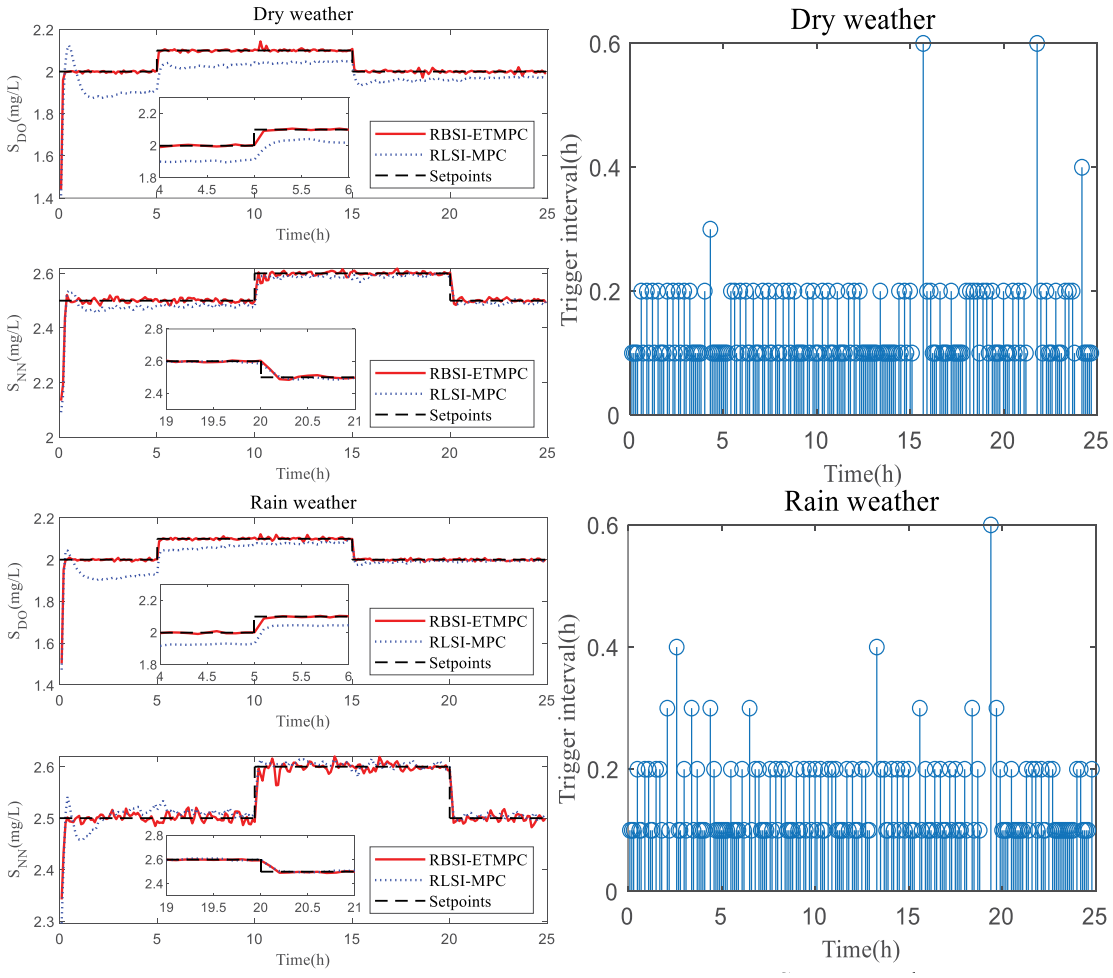

Fig. 7 (Continued)

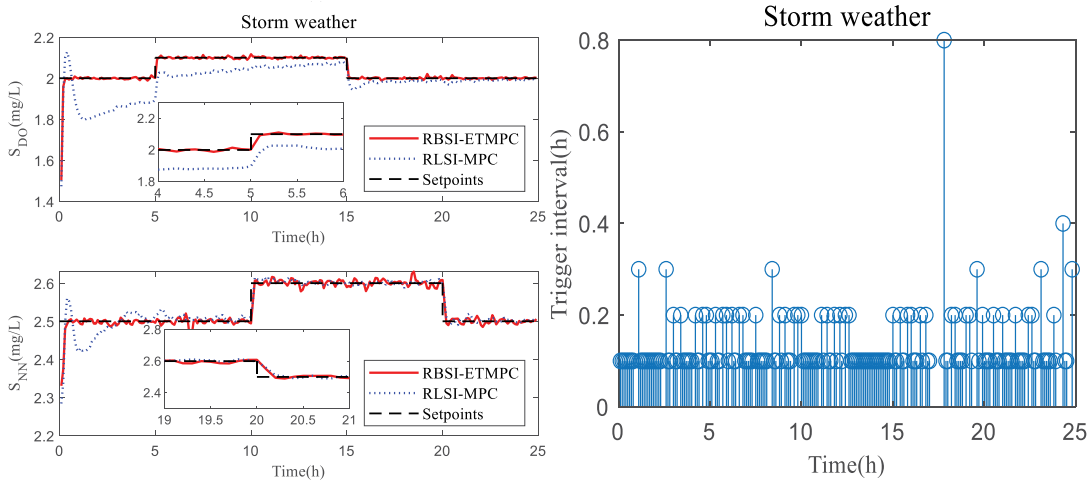

Fig. 7. Control effects of RBSI-ETMPC with variable setpoints under three working conditions.

Table 3
Control accuracy of different control strategies with variable setpoints under three working conditions

Working condition	Variable	Controller	IAE (mg/L)	ISE (mg/L)	DEV^{max} (mg/L)
Dry weather	$S_{DO,5}$	RBSI-ETMPC	3.99×10^{-3}	4.01×10^{-5}	4.31×10^{-2}
		RLSI-MPC	5.14×10^{-2}	2.96×10^{-3}	1.18×10^{-1}
		LSI-MPC	7.71×10^{-2}	7.25×10^{-3}	2.65×10^{-1}
	$S_{NN,2}$	RBSI-ETMPC	5.70×10^{-3}	7.70×10^{-5}	4.98×10^{-2}
		RLSI-MPC	1.27×10^{-2}	2.20×10^{-4}	6.74×10^{-2}
		LSI-MPC	7.34×10^{-2}	1.46×10^{-2}	3.74×10^{-1}
Rain weather	$S_{DO,5}$	RBSI-ETMPC	3.61×10^{-3}	2.40×10^{-5}	2.19×10^{-2}
		RLSI-MPC	2.10×10^{-2}	7.10×10^{-4}	7.79×10^{-2}
		LSI-MPC	6.28×10^{-2}	7.24×10^{-3}	2.32×10^{-1}
	$S_{NN,2}$	RBSI-ETMPC	6.45×10^{-3}	9.20×10^{-5}	5.06×10^{-2}
		RLSI-MPC	7.44×10^{-3}	9.20×10^{-5}	4.25×10^{-2}
		LSI-MPC	3.29×10^{-2}	1.85×10^{-3}	9.72×10^{-2}
Storm weather	$S_{DO,5}$	RBSI-ETMPC	3.37×10^{-3}	2.18×10^{-5}	2.09×10^{-2}
		RLSI-MPC	3.61×10^{-2}	2.00×10^{-3}	1.13×10^{-1}
		LSI-MPC	8.04×10^{-2}	1.14×10^{-2}	2.83×10^{-1}
	$S_{NN,2}$	RBSI-ETMPC	6.50×10^{-3}	9.59×10^{-5}	4.87×10^{-2}
		RLSI-MPC	6.45×10^{-3}	8.90×10^{-5}	5.74×10^{-2}
		LSI-MPC	2.54×10^{-2}	1.34×10^{-3}	9.13×10^{-2}

Fig. 8 shows the control effect of the RBSI-ETMPC with variable setpoints and input pulse interference under three working conditions. Fig. 8 demonstrates that RBSI-ETMPC can not only track the setpoints in a short time but also respond to step changes quickly. In addition, when input pulse interference is applied, RBSI-ETMPC can overcome the interference and quickly stabilize at the setpoints. Compared with RLSI-MPC, the proposed RBSI-ETMPC has high steady-state control accuracy. Under the action of the event-triggering strategy, the longest trigger interval is 0.3 h, showing that the proposed RBSI-ETMPC can effectively reduce the number of control actions.

Table 4 gives the values of the IAE, ISE and DEV^{max} for different control strategies. Compared with RLSI-MPC and LSI-MPC, the proposed RBSI-ETMPC can significantly reduce the number of actions and save the limited control resources without reducing the control performance. Taking storm weather conditions as an example, for the control of $S_{DO,5}$, compared with RLSI-MPC, the values of the IAE, ISE and DEV^{max} of RBSI-ETMPC decreased by 85.09%, 76.82% and 29.62%, respectively. For the control of $S_{NN,2}$, compared with RLSI-MPC and LSI-MPC, the values of IAE and ISE of RBSI-ETMPC decreased slightly.

4.3.5. Variable setpoint control with output pulse interference (Experiment 5)

In the experiment of variable setpoint control with output pulse interference for the WWTP, the settings of the concentration of $S_{DO,5}$ and the level of $S_{NN,2}$ are the same as

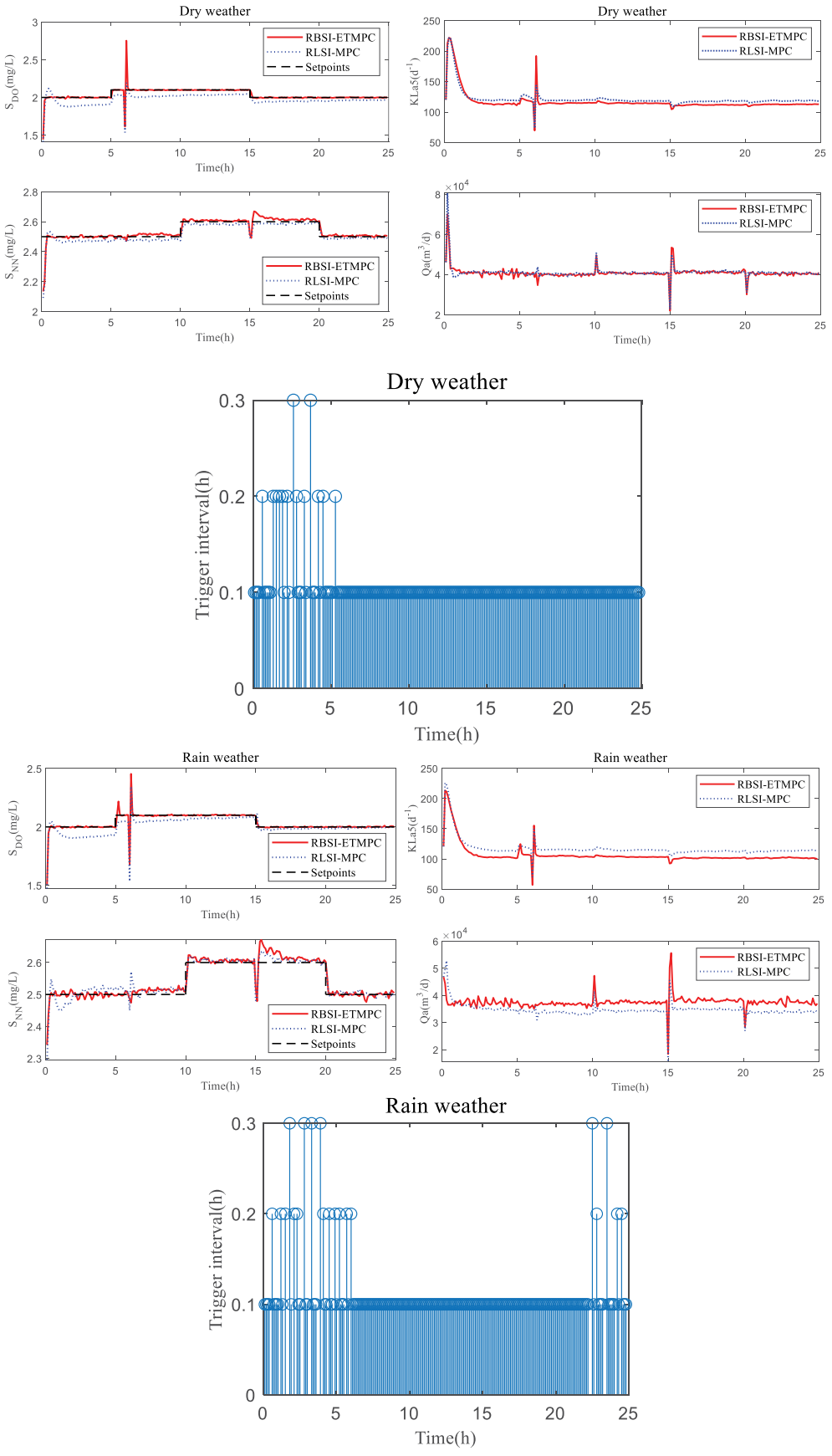

Fig. 8 (Continued)

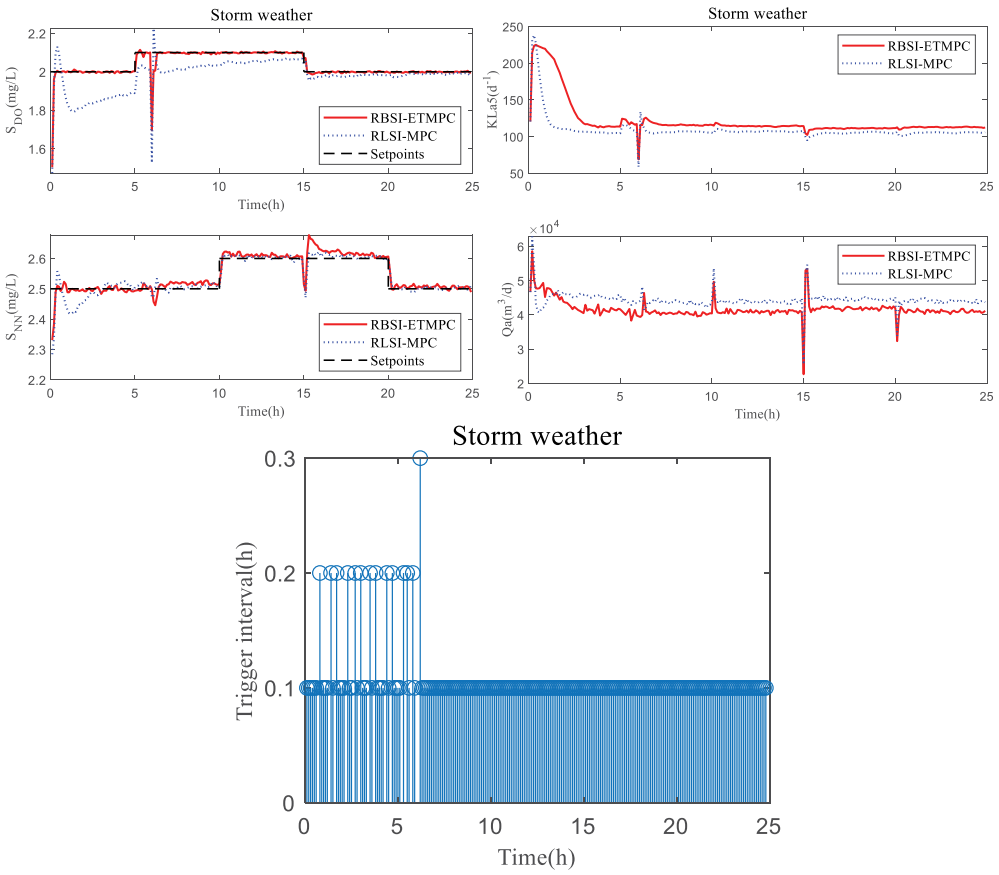

Fig. 8. Control effects of RBSI-ETMPC with variable setpoints under three working conditions.

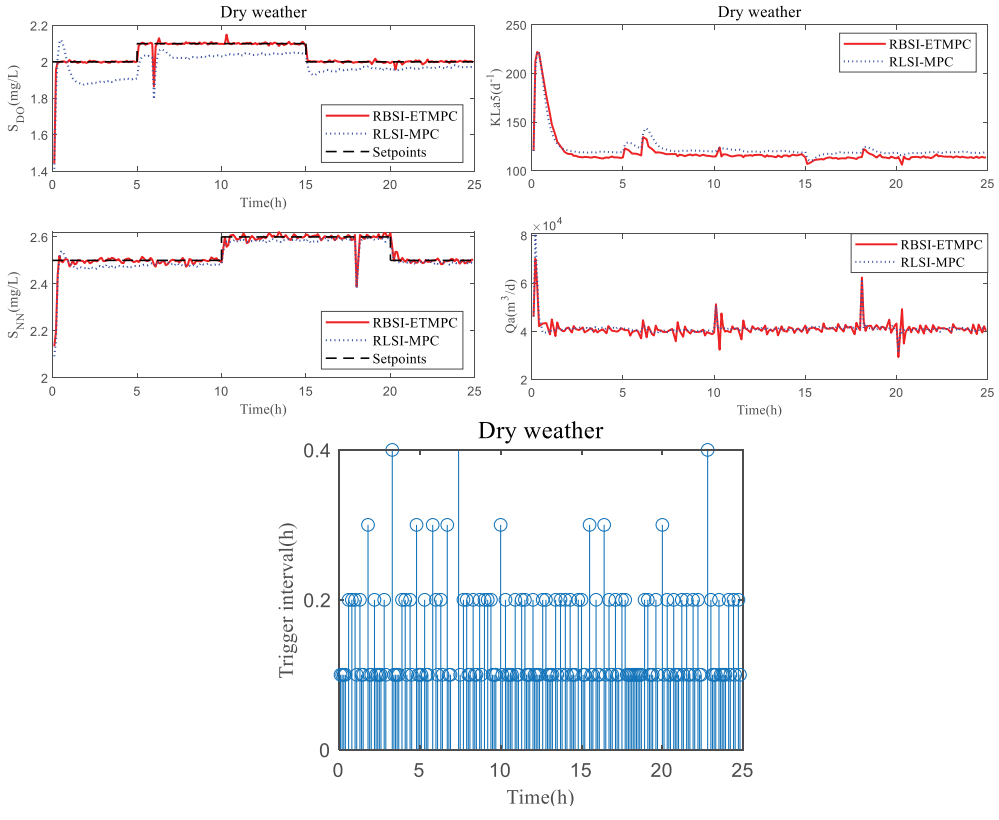

Fig. 9 (Continued)

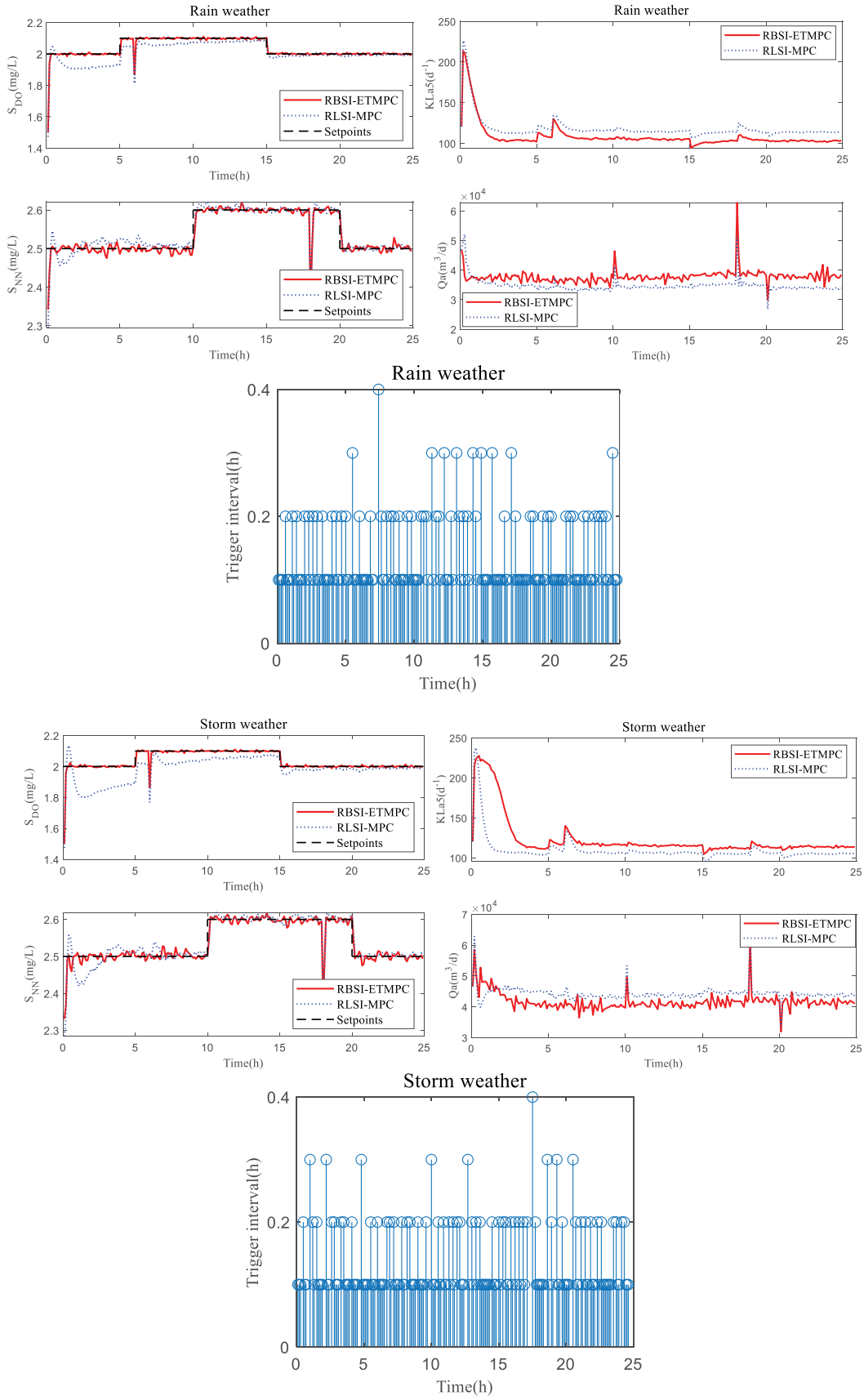

Fig. 9. Control effects of RBSI-ETMPC with variable setpoints under three working conditions.

Table 4
Control accuracy of different control strategies with variable setpoints under three working conditions

Working condition	Variable	Controller	IAE (mg/L)	ISE (mg/L)	DEV^{max} (mg/L)
Dry weather	$S_{DO,5}$	RBSI-ETMPC	8.96×10^{-3}	3.35×10^{-3}	6.53×10^{-1}
		RLSI-MPC	6.22×10^{-2}	5.47×10^{-3}	5.63×10^{-1}
		LSI-MPC	1.09×10^{-1}	1.41×10^{-2}	3.86×10^{-1}
	$S_{NN,2}$	RBSI-ETMPC	1.28×10^{-2}	3.52×10^{-4}	1.09×10^{-1}
		RLSI-MPC	1.60×10^{-2}	4.00×10^{-4}	1.07×10^{-1}
		LSI-MPC	1.28×10^{-1}	2.49×10^{-2}	3.69×10^{-1}
Rain weather	$S_{DO,5}$	RBSI-ETMPC	7.29×10^{-3}	1.60×10^{-3}	4.21×10^{-1}
		RLSI-MPC	2.86×10^{-2}	2.85×10^{-3}	5.66×10^{-1}
		LSI-MPC	6.91×10^{-2}	9.22×10^{-3}	6.44×10^{-1}
	$S_{NN,2}$	RBSI-ETMPC	1.24×10^{-2}	3.78×10^{-4}	1.21×10^{-1}
		RLSI-MPC	1.03×10^{-2}	3.20×10^{-4}	1.20×10^{-1}
		LSI-MPC	7.42×10^{-2}	7.18×10^{-3}	3.22×10^{-1}
Storm weather	$S_{DO,5}$	RBSI-ETMPC	6.47×10^{-3}	9.55×10^{-4}	4.04×10^{-1}
		RLSI-MPC	4.34×10^{-2}	4.12×10^{-3}	5.74×10^{-1}
		LSI-MPC	7.83×10^{-2}	1.25×10^{-2}	6.42×10^{-1}
	$S_{NN,2}$	RBSI-ETMPC	1.48×10^{-2}	4.27×10^{-4}	1.06×10^{-1}
		RLSI-MPC	8.60×10^{-3}	2.20×10^{-4}	1.29×10^{-1}
		LSI-MPC	9.11×10^{-2}	1.26×10^{-2}	2.66×10^{-1}

Table 5
Control accuracy of different control strategies with variable setpoints under three working conditions

Working condition	Variable	Controller	IAE (mg/L)	ISE (mg/L)	DEV^{max} (mg/L)
Dry weather	$S_{DO,5}$	RBSI-ETMPC	5.14×10^{-3}	3.21×10^{-4}	2.34×10^{-1}
		RLSI-MPC	5.30×10^{-2}	3.47×10^{-3}	3.06×10^{-1}
		LSI-MPC	2.73×10^{-2}	2.54×10^{-3}	2.62×10^{-1}
	$S_{NN,2}$	RBSI-ETMPC	9.00×10^{-3}	4.01×10^{-4}	2.11×10^{-1}
		RLSI-MPC	1.48×10^{-2}	5.20×10^{-4}	2.19×10^{-1}
		LSI-MPC	8.80×10^{-2}	1.39×10^{-2}	3.73×10^{-1}
Rain weather	$S_{DO,5}$	RBSI-ETMPC	4.43×10^{-3}	2.86×10^{-4}	2.32×10^{-1}
		RLSI-MPC	2.19×10^{-2}	1.09×10^{-3}	2.90×10^{-1}
		LSI-MPC	1.17×10^{-1}	2.22×10^{-2}	4.32×10^{-1}
	$S_{NN,2}$	RBSI-ETMPC	7.14×10^{-3}	4.02×10^{-4}	2.36×10^{-1}
		RLSI-MPC	8.70×10^{-3}	4.40×10^{-4}	2.43×10^{-1}
		LSI-MPC	1.67×10^{-1}	3.79×10^{-2}	3.75×10^{-1}
Storm weather	$S_{DO,5}$	RBSI-ETMPC	4.36×10^{-3}	2.95×10^{-4}	2.35×10^{-1}
		RLSI-MPC	3.76×10^{-2}	2.52×10^{-3}	3.34×10^{-1}
		LSI-MPC	1.23×10^{-1}	2.86×10^{-2}	4.65×10^{-1}
	$S_{NN,2}$	RBSI-ETMPC	8.05×10^{-3}	4.26×10^{-4}	2.36×10^{-1}
		RLSI-MPC	9.24×10^{-3}	4.50×10^{-4}	2.25×10^{-1}
		LSI-MPC	1.77×10^{-1}	5.16×10^{-2}	5.07×10^{-1}

those in Experiment 2. However, output pulse interferences are added to $S_{DO,5}$ at 6 h and to $S_{NN,2}$ at 18 h. The control parameter settings of the RBSI-ETMPC in this experiment are the same as those in Experiment 2.

Fig. 9 shows the control effect of the RBSI-ETMPC controller with variable setpoints and output pulse interference under three working conditions. Fig. 9 shows that RBSI-ETMPC has superior control performance. In particular, when pulse interference occurs in the output, RBSI-ETMPC can suppress the adverse effects of interference by adaptively adjusting the control quantity. Compared with RLSI-MPC, the control stability and accuracy of the proposed RBSI-ETMPC have been significantly improved. Under the complex working conditions of storm weather, the designed RBSI-ETMPC controller has a slight oscillation phenomenon for the control of $S_{NN,2}$ due to the introduction of an

event-triggering strategy. From Fig. 9, the longest trigger interval is 0.4 h, which shows that the event trigger strategy can effectively save computing resources.

Table 5 presents the values of the IAE, ISE and DEV^{max} for different control strategies. Compared with RLSI-MPC and LSI-MPC, the proposed RBSI-ETMPC has a smaller IAE, ISE and DEV^{max} under the three working conditions, which indicates that it can adapt well to the variable setpoints and output pulse interference. Taking rain weather conditions as an example, for the control of $S_{DO,5}$, compared with RLSI-MPC, the values of IAE, ISE and DEV^{max} of RBSI-ETMPC decreased by 79.77%, 73.76% and 25.00%, respectively. For the control of $S_{NN,2}$, compared with RLSI-MPC, the values of IAE, ISE and DEV^{max} of RBSI-ETMPC decreased by 21.85%, 8.64% and 2.88%, respectively.

5. Conclusion

Aiming at the precise control of dissolved oxygen and nitrate nitrogen in the biochemical reaction process of municipal wastewater treatment, this paper proposes an event-triggered predictive control strategy based on recursive bilinear subspace identification. The designed recursive bilinear subspace identification method with a forgetting factor can not only obtain the precise state space model of the controlled object but also update the model parameters recursively online to enhance the adaptability of the model. The predictive control strategy with an event-triggering mechanism can not only overcome the defect that the post-event control cannot actively suppress the control error but also avoid unnecessary control operations, thus enhancing the control performance and reducing the control energy consumption. In this paper, the BSM1 model is used for simulation verification. Four experimental cases, including multivariable constant value control, multivariable variable setpoint control, variable setpoint control with input pulse interference, and variable setpoint control with output pulse interference, are designed under three complex working conditions. The predictive performance verification of the RBSI model and the control performance verification of the RBSI-ETMPC controller are completed. The experimental results clearly show the superior performance of the proposed RBSI-ETMPC, which lays a foundation for its successful application in wastewater treatment plants.

To enhance the capability of the model to depict complex dynamic systems, the next step is to establish a prediction model for MPC using neural networks. Structural identification and parameter estimation are two critical issues that need to be addressed carefully for neural network-based prediction models. Therefore, the introduction of a parameter adaptive learning mechanism and a structure self-organization adjustment mechanism can improve the identification ability of neural networks. In addition, combining advanced algorithms such as deep learning, reinforcement learning, and brain-like computing can improve the learning ability of the model. It is worth mentioning that the computational complexity of real-time control rates for neural network-based MPC will increase greatly. Researchers can attempt to acquire control rates online using gradient descent algorithms, LM and its variants, and neural dynamics optimization methods.

At the same time, to break through the basic theories and methods required for the construction of unattended wastewater treatment plants, optimization algorithms, such as multi-objective optimization, constrained multi-objective optimization, and dynamic multi-objective optimization, can be used to obtain the optimal setpoints of dissolved oxygen and nitrate nitrogen.

Acknowledgements

The authors would like to thank the reviewers and the editors for their valuable suggestions and contributions, which significantly helped to improve this article. This work was supported by the Industry University Research Cooperation Project of Jiangsu Province (Grant number BY2020247), the Postgraduate Research & Practice Innovation Program of Jiangsu Province (Grant No. SJCX23_1855), and the Innovation and Entrepreneurship Training Program for College Students of Jiangsu Province (Grant numbers 202211049074Y and 202211049125H).

Author contributions

Hongbiao Zhou: conceptualization, methodology, funding acquisition, resources, reviewing and editing; Shuaixiang Liu: software, formal analysis, writing of the original draft; Jian Ren: software; Jinlong Zhang: data curation; Honghai Li: reviewing and editing.

References

[1] L. Wang, W. Gu, Y. Liu, P. Liang, X. Zhang, X. Huang, Challenges, solutions and prospects of mainstream anammox-based process for municipal wastewater treatment, Sci. Total Environ., 820 (2022) 153351, doi: 10.1016/j.scitotenv.2022.153351.
[2] M. Molinos-Senante, A. Maziotis, Evaluation of energy efficiency of wastewater treatment plants: the influence of the technology and aging factors, Appl. Energy, 310 (2022) 118535, doi: 10.1016/j.apenergy.2022.118535.
[3] D. Selișteanu, I.-M. Popescu, M. Roman, C. Șulea-Iorgulescu, S. Mehedințeanu, A software emulator for the modelling and control of an activated sludge process in a wastewater treatment plant, Processes, 9 (2021) 2054, doi: 10.3390/pr9112054.
[4] S. Du, Q. Yan, J. Qiao, Event-triggered PID control for wastewater treatment plants, J. Water Process Eng., 38 (2020) 101659, doi: 10.1016/j.jwpe.2020.101659.
[5] X. Song, Y. Zhao, Z. Song, C. Liu, Dissolved oxygen control in wastewater treatment based on robust PID controller, Int. J. Model. Identif., 15 (2012) 297–303.
[6] K. Saravana, K. Latha, A supervisory fuzzy logic control scheme to improve effluent quality of a wastewater treatment plant, J. Water Process Eng., 84 (2021) 3415–3424.
[7] W. Zhang, J. Qiao. Multi-variable direct self-organizing fuzzy neural network control for wastewater treatment process, Asian J. Control, 22 (2020) 716–728.
[8] J. Qiao, G. Han, H. Han, C. Yang, W. Li, Decoupling control for wastewater treatment process based on recurrent fuzzy neural network, Asian J. Control, 21 (2019) 1270–1280.
[9] W. Wei, N. Chen, Z. Zhang, Z. Liu, M. Zuo, U-model-based active disturbance rejection control for the dissolved oxygen in a wastewater treatment process, Math. Probl. Eng., 2020 (2020) 3507910, doi: 10.1155/2020/3507910.
[10] S. Zhang, P. Zhou, Y. Xie, T. Chai, Improved model-free adaptive predictive control method for direct data-driven control of a wastewater treatment process with high performance, J. Process Control, 110 (2022) 11–23.

[11] W. Wei, N. Chen, Z. Zhang, Z. Liu, M. Zuo, K. Liu, Y. Xia, A scalable-bandwidth extended state observer-based adaptive sliding-mode control for the dissolved oxygen in a wastewater treatment process, IEEE Trans. Cybern., 52 (2021) 13448–13457.
[12] J. Berberich, J. Köhler, M.A. Müller, F. Allgöwer, Data-driven model predictive control with stability and robustness guarantees, IEEE Trans. Autom. Control, 66 (2020) 1702–1717.
[13] B. Holenda, E. Domokos, A. Redey, J. Fazakas, Dissolved oxygen control of the activated sludge wastewater treatment process using model predictive control, Comput. Chem. Eng., 32 (2008) 1270–1278.
[14] M.A. Brdys, M. Grochowski, T. Gminski, K. Konarczak, M. Drewa, Hierarchical predictive control of integrated wastewater treatment systems, Control Eng. Pract., 16 (2008) 751–767.
[15] W. Shen, X. Chen, J.P. Corriou, Application of model predictive control to the BSM1 benchmark of wastewater treatment process, Comput. Chem. Eng., 32 (2008) 2849–2856.
[16] M. Mulas, S. Tronci, F. Corona, H. Haimi, P. Lindell, M. Heinonen, R. Baratti, Predictive control of an activated sludge process: an application to the Viikinmäki wastewater treatment plant, J. Process Control, 35 (2015) 89–100.
[17] W. Shen, X. Chen, M.N. Pons, J.P. Corriou, Model predictive control for wastewater treatment process with feedforward compensation, Chem. Eng. J., 155 (2009) 161–174.
[18] N. Boruah, B.K. Roy, Event triggered non-linear model predictive control for a wastewater treatment plant, J. Water Process Eng., 32 (2019) 100887, doi: 10.1016/j.jwpe.2019.100887.
[19] S, Du, Q. Zhang, H. Han, H. Sun, J. Qiao, Event-triggered model predictive control of wastewater treatment plants, J. Water Process Eng., 47 (2022) 102765, doi: 10.1016/j.jwpe.2022.102765.
[20] H. Han, S. Fu, H. Sun, C. Qin, J. Qiao, Modeling and control of wastewater treatment process with time delay based on event-triggered recursive least squares, Eng. Appl. Artif. Intell., 122 (2023) 106052, doi: 10.1016/j.engappai.2023.106052.
[21] H. Han, J. Qiao, Non-linear model-predictive control for industrial processes: an application to wastewater treatment process, IEEE Trans. Ind. Electron., 61 (2013) 1970–1982.
[22] H. Han, H. Qian, J. Qiao, Non-linear multiobjective model-predictive control scheme for wastewater treatment process, J. Process Control, 24 (2014) 47–59.
[23] H. Han, Z. Liu, Y. Hou, J. Qiao, Data-driven multiobjective predictive control for wastewater treatment process, IEEE Trans. Ind. Electron., 16 (2019) 2767–2775.
[24] H. Han, S. Fu, H. Sun, J. Qiao, Hierarchical non-linear model predictive control with multi-time-scale for wastewater treatment process, J. Process Control, 108 (2021) 125–135.
[25] P.B. Cox, R. Tóth, Linear parameter-varying subspace identification: a unified framework, Automatica, 123 (2021) 109296, doi: 10.1016/j.automatica.2020.109296.
[26] M. Jalanko, Y. Sanchez, V. Mahalec, P. Mhaskar, Adaptive system identification of industrial ethylene splitter: a comparison of subspace identification and artificial neural networks, Comput. Chem. Eng., 147 (2021) 107240, doi: 10.1016/j.compchemeng.2021.107240.
[27] E.P. Reynders, Uncertainty quantification in data-driven stochastic subspace identification, Mech. Syst. Signal Process., 151 (2021) 107338, doi: 10.1016/j.ymssp.2020.107338.
[28] S. Qin, An overview of subspace identification, Comput. Chem. Eng., 30 (2006) 1502–1513.
[29] P. Zhou, S. Zhang, P. Dai, Recursive learning-based bilinear subspace identification for online modeling and predictive control of a complicated industrial process, IEEE Access, 8 (2020) 62531–62541.
[30] V. Vajpayee, S. Mukhopadhyay, A.P. Tiwari, Data-driven subspace predictive control of a nuclear reactor, IEEE Trans. Nucl. Sci., 65 (2017) 666–679.
[31] Al. Hasnain, F. Sahami, S. Kamalasadan, An online wide-area direct coordinated control architecture for power grid transient stability enhancement based on subspace identification, IEEE Trans. Ind. Appl., 57 (2021) 2896–2907.
[32] Q. Chen, H. Sheng, T. Zhang, A novel direct performance adaptive control of aero-engine using subspace-based improved model predictive control, Aerosp. Sci. Technol., 128 (2022) 107760, doi: 10.1016/j.ast.2022.107760.
[33] X. Luo, Y. Song, Data-driven predictive control of Hammerstein–Wiener systems based on subspace identification, Inf. Sci., 422 (2018) 447–461.
[34] Z. Li, X. Yuan, Y. Wang, C. Xie, Subspace predictive control with the data-driven event-triggered law for linear time-invariant systems, J. Franklin Inst., 356 (2019) 8167–8181.
[35] M. Ahmadipour, S.R. Seydnejad, M. Barkhordari-Yazdi, Subspace-based deterministic identification of MIMO linear state-delayed systems, Circuits Syst. Signal Process., 39 (2020) 4067–4093.
[36] P. Zhou, H. Song, H. Wang, T. Chai, Data-driven non-linear subspace modeling for prediction and control of molten iron quality indices in blast furnace ironmaking, IEEE Trans. Control Syst. Technol., 25 (2016) 1761–1774.
[37] N. Patel, J. Nease, S. Aumi, C. Ewaschuk, J. Luo, P. Mhaskar, Integrating data-driven modeling with first-principles knowledge, Ind. Eng. Chem. Res., 59 (2020) 5103–5113.
[38] N. Patel, B. Corbett, P. Mhaskar, Model predictive control using subspace model identification, Comput. Chem. Eng., 149 (2021) 107276, doi: 10.1016/j.compchemeng.2021.107276.
[39] D. Ghosh, E. Hermonat, P. Mhaskar, S. Snowling, R. Goel, Hybrid modeling approach integrating first-principles models with subspace identification, Ind. Eng. Chem. Res., 58 (2019) 13533–13543.
[40] H. Zhou, J. Qiao, Multiobjective optimal control for wastewater treatment process using adaptive MOEA/D, Appl. Intell., 49 (2019) 1098–1126.
[41] R. Yang, D. Wang, J. Qiao, Policy gradient adaptive critic design with dynamic prioritized experience replay for wastewater treatment process control, IEEE Trans. Ind. Inf., 18 (2021) 3150–3158.
[42] H. Han, H. Liu, J. Li, J. Qiao, Cooperative fuzzy-neural control for wastewater treatment process, IEEE Trans. Ind. Inf., 17 (2020) 5971–5981.